ACS APPLIED MATERIALS & INTERFACES

Research Article

www.acsami.org

Nano-hydroxyapatite and Nano-titanium Dioxide Exhibit Different Subcellular Distribution and Apoptotic Profile in Human Oral Epithelium

Chor Yong Tay,[†,§] Wanru Fang,[†,‡,§] Magdiel Inggrid Setyawati,[†] Sing Ling Chia,[†] Kai Soo Tan,[‡] Catherine Hsu Ling Hong,*[,‡] and David Tai Leong*[,†]

[†]Department of Chemical and Biomolecular Engineering, National University of Singapore, 4 Engineering Drive 4, Singapore 117585, Singapore

[‡]Faculty of Dentistry, National University of Singapore, 5 Lower Kent Ridge Road, Singapore 119083, Singapore

ABSTRACT: Nanomaterials (NMs) such as titanium dioxide (nano-TiO_2) and hydroxyapatite (nano-HA) are widely used in food, personal care, and many household products. Due to their extensive usage, the risk of human exposure is increased and may trigger NMs specific biological outcomes as the NMs interface with the cells. However, the interaction of nano-TiO_2 and nano-HA with cells, their uptake and subcellular distribution, and the cytotoxic effects are poorly understood. Herein, we characterized and examined the cellular internalization, inflammatory response and cytotoxic effects of nano-TiO_2 and nano-HA using TR146 human oral buccal epithelial cells as an in vitro model. We showed both types of NMs were able to bind to the cellular membrane and passage into the cells in a dose dependent manner. Strikingly, both types of NMs exhibited distinct subcellular distribution profile with nano-HA displaying a higher preference to accumulate near the cell membrane compared to nano-TiO_2. Exposure to both types of NMs caused an elevated reactive oxygen species (ROS) level and expression of inflammatory transcripts with increasing NMs concentration. Although cells treated with nano-HA induces minimal apoptosis, nano-TiO_2 treated samples displayed approximately 28% early apoptosis after 24 h of NMs exposure. We further showed that nano-TiO_2 mediated cell death is independent of the classical p53-Bax apoptosis pathway. Our findings provided insights into the potential cellular fates of human oral epithelial cells as they interface with industrial grade nano-HA and nano-TiO_2.

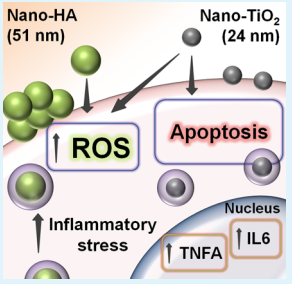

KEYWORDS: *nanomaterials, nanotoxicology, oral mucosa, reactive oxidative stress, inflammation*

1. INTRODUCTION

In the past decade, the field of nanotechnology has matured considerably to the extent that manufactured nanomaterials (NMs) can be produced on an industrial scale basis with high consistency and be incorporated to wide spectrum of consumer products to improve the economics and performance of the products. Because the NMs are of comparable length scale as discrete components and proteins that makes up a cell, NMs may potentially evade the cellular defense mechanism leading to permanent cell injury.[1−3] With the prevalence of NMs being incorporated in off-the-shelf products, our exposure to NMs will correspondingly increase. Consequently, the interaction of NMs with biological systems such as living cells has become one of the most fascinating areas of science and applied research that lies at the interface of nanotechnology and biology.[4,5] Nanoscale hydroxyapatite (nano-HA) and titanium dioxide (nano-TiO_2) are among the many NMs that are intentionally added into oral hygiene products.[6] Nano-HA resembles tooth enamel[7] and can restore the enamel layer and treat tooth hypersensitivity and increase enamel's resistance to dental decay.[8] On the other hand, nano-TiO_2 is used extensively in personal care products as a bright white pigment in toothpaste. Recent studies have shown that both nano-HA and nano-TiO_2 are capable of inducing considerable cytotoxic effects to a variety of mammalian cell lines.[9−11] However, the potential health impact that may be introduced by these NMs, especially in the oral milieu remains unclear to date. A better understanding into the kind of biological responses nano-HA and nano-TiO_2 may elicit, will allow us to devise strategies to manage or minimize NMs related risks.

Unlike the epidermal lining of other organs such as the skin, the nonkeratinized oral mucosa epithelium is significantly more permeable.[12] Permeability of the oral epithelium lining region such as the inner cheeks, inner lips and floor of the tongue may be further enhanced under the influence of alcohol and surfactant such as sodium dodecyl sulfate that are commonly found in oral care products.[13,14] Furthermore, trauma injury induced lesions (e.g., ulcers) to the oral mucosa layer may compromise the protective barrier and facilitate entry of NMs into the deep tissue.[15] It is not improbable that NMs can traverse and affect the oral mucosa cells' physiology.[16] These NMs might even enter the blood circulation and possibly lead to systemic exposure.[17]

Received: August 29, 2013
Accepted: April 15, 2014
Published: April 15, 2014

The pervasive use of toothpastes in oral hygiene on a chronic regime in human populations, then argues for the importance of studying the impact of NMs found in commercially available toothpastes on fundamental biological functions of the human buccal epithelium. In this study, nano-HA (~51 nm) and nano-TiO_2 (~24 nm), two common additives found in oral hygiene products were employed to elucidate its effects on TR146 human oral mucosa epithelial cells.[6,18] Preferential accumulation of nano-HA in the cell membrane was observed in TR146 relative to nano-TiO_2. Both types of NMs were able to induce significantly higher generation of intracellular ROS in a dose-dependent manner. Furthermore, NMs treatment was sufficient to upregulate expression of inflammatory transcripts such as IL6 and TNFA, suggesting that NMs may potentiate inflammation. However, only cells treated with nano-TiO_2 but not nano-HA were observed to have undergone significant apoptosis that does not involve the p53-Bax pathway. Our findings imply that both nano-HA and nano-TiO_2 are capable of eliciting varying degree of detrimental acute cellular responses in TR146 oral epithelial cells, providing vital insights into the potential fate of cells in the oral milieu as they interface with nano-HA and nano-TiO_2.

2. EXPERIMENTAL DETAILS

2.1. Preparation and Physical Characterization of NMs. Nano-HA particles were purchased from Sigma-Aldrich, U.S.A., and nano-TiO_2 particles (AEROXIDE P25) were purchased from Evonik Degussa, U.S.A. Stock solution of 125 mM of both NMs was prepared in ultrapure water. Probe sonication (Micron TM XL 2000, Qsonica, U.S.A.) was applied to the NM solution for 30 s before diluting in the various desired dispersants. Nano-HA and nano-TiO_2 resuspended in ethanol (50 μg/mL) were viewed using transmission electron microscopy (TEM) (JEOL JEM-2010, Japan). The NMs primary particle size was determined by scoring 50 randomly chosen NMs using ImageJ software. Hydrodynamic size and ζ-potential of the NMs was determined in DMEM/F12 complete culture medium supplemented with 10% FBS and 1% penicillin/streptomycin solution using the Zeta Nanosizer (Malvern Co, U.K.).

2.2. Conjugation of NMs with FITC Fluorescent Probe. NMs were first dispersed in anhydrous ethanol (Fisher Scientific, U.S.A.); thereafter, 5% v/v of 3-Aminopropyltriethoxysilane (APTES; Sigma-Aldrich, USA) was added dropwise to the suspension and stirred continuously at 80 °C for 5 h. To the APTES treated NMs, fluorescein isothiocyanate (FITC; Sigma-Aldrich, U.S.A.) at a concentration of 0.25−0.5 g/mL was added and the mixture was stirred continuously for an additional 16 h at 80 °C in dark. At the end of the reaction, FITC tagged NMs were centrifuged at 6000 rpm for 20 min and washed with ethanol followed by water for 5 times before the FITC-NMs were freeze-dried and stored at room temperature in the dark to minimize photobleaching.

2.3. Cell Culture. Human buccal epithelial cells (TR146; Sigma-Aldrich, U.S.A.) was cultured in 1:1 complete high glucose Dulbecco's Modified Eagle's Media: nutrient mixture F-12(DMEM/F12) (Invitrogen, MA, U.S.A.) and supplemented with 10% fetal bovine serum (FBS) under standard culture condition of 37 °C, 5% CO_2. Cell medium were replenished every 2−3 days of culture.

2.4. Membrane and Cytosolic Localized NMs Content Extraction. TR146 cells were plated overnight at plating density of 30 000 cells/cm^2. 125 and 1250 μM of FITC-NMs in DMEM/F12 (1:1) complete medium were introduced to the cells for a further 12 h before the NMs treated cells were washed and the membrane and cytosolic contents were fractionated (Mem-PER Eukaryotic Extraction Kit; Thermo Scientific, U.S.A.). The extracted membrane and cytosolic fractions were collected and fluorescence measurements were made at an excitation/emission wavelength of 488/520 nm using the microplate reader (Tecan Infinite 200, Tecan Inc., Switzerland).

2.5. Confocal Microscopy. TR146 epithelial cells were seeded on coverslips (Menzel-Gläser, Germany) at 30 000 cells/cm^2 overnight under standard culture condition. To label the cell body, cells were incubated with 1 μM of CellTracker Red CMTPX (Molecular Probes, U.S.A.) in serum free DMEM/F12 for 1 h at 37 °C. Following which, the cells were washed 3 times with PBS and treated with FITC-NMs at a concentration of 1250 μM for 12 h at 37 °C in complete cell culture medium. At the end of the incubation duration, the cells were then washed 3 times with PBS to remove any unbound FITC-NMs. Cell nuclei were stained with Hoechst 33342 (1 μg/mL, Molecular Probes, U.S.A.) for 15 min at 37 °C in complete cell culture medium, washed 3 times and fresh medium was reintroduced to the cells. Cells were examined under a Nikon A1 confocal microscope using a 100× objective (NA of 1.4) and a 1× zoom. The three-dimensional (3D) structure of the nanoparticles treated cells was reconstructed and analyzed using the Nikon NIS-element AR software.

2.6. Intracellular Reactive Oxygen Species (ROS) Level Measurement. TR146 epithelial cells (30 000 cells/cm^2) were first grown overnight before the media was replaced with media containing different concentrations of NMs (0, 62.5, 125, 250, 500, and 1250 μM). Following 24 h of NMs treatment, the intracellular ROS level was detected and measured using 10 μM of 2′,7′-dichlorofluorescin diacetate (DCFH-DA; Sigma-Aldrich, U.S.A.). ROS level was normalized against the amount of DNA in each sample using Hoechst 33342 (Molecular Probes, U.S.A.). The DCF and Hoechst dye intensity were detected with excitation/emission wavelengths of 488/525 nm and 350/461 nm, respectively. The fluorescence intensity of each fluorophore was measured using a microplate reader. Microplate reader (Infinite 200 Pro, Tecan, Switzerland). Data obtained represents the mean values of three independent experiments. To detect mitochondrial specific superoxide, using the same NMs exposure regime, the cells were subsequently counterstained with 2.5 μM of MitoSox Red (Molecular Probes, U.S.A.) in accordance to the protocol provided by the manufacturer. The cells were then detached using trypsin, centrifuged, resuspended in PBS and analyzed using the Tali image cytometer (Invitrogen, U.S.A.). Cells treated with 1 mM of H_2O_2 at 37 °C for 4 h were used as positive control.

2.7. Expression Level of Inflammatory Response Genes. TR146 cells were exposed to various concentrations of NMs for 24 h after which, total RNA was isolated using RNeasy Mini kit (Qiagen, Germany). RNA was reversed transcribed to cDNA using RevertAid H Minus First Strand cDNA synthesis (Fermentas, U.S.A.). Quantitative PCR reactions were performed on a ABI 7300 real-time PCR system (Applied Biosystem, U.S.A.). Human TATA-box binding protein (hTBP) was used as an internal control. The sequences of the forward and reverse primers for various genes assessed are as listed: TNFA forward 5′ CCT CTC TCT AAT CAG CCC TCTG 3′; TNFA reverse 5′ GAG GAC CTG GGA GTA GAT GAG 3′; IL6 forward 5′ GAA AGC AGC AAA GAG GCA CT 3′ IL6 reverse 5′ TTT CAC CAG GCA AGT CTC CT 3′; hTBP forward 5′ TGC CCG AAA CGC CGA ATA TAA TC 3′ hTBP reverse 5′ GTC TGG ACT GTT CTT CAC TCT TGG 3′.

2.8. Measurement of NF-κB Secreted. RAW 264.7 cells were stably transfected with NF-κB-SEAP (secreted embryonic alkaline phosphatase) reporter gene (Kind gift from Dr. Kai Soo TAN). RAW 264.7-NF-κB-SEAP cells were treated with 0, 62.5, 125, 250, 500, and 1250 μM of nano-HA and nano-TiO_2 for 6 h. SEAP was detected via Phospha-Light SEAP reporter gene assay (Applied Biosystem, U.S.A.). Chemiluminescence signal was detected using a luminometer (Glomax 96 well microplate luminometer, Promega)

2.9. Cell Apoptosis and Signaling Assays. After NMs treatment, the percentage of apoptotic cells was determined by use of flow cytometry (MUSE cell analyzer, Merck Millipore, U.S.A.). Cells pellets were collected via trypsinization and centrifugation before it was resuspended in solution containing Annexin V-FITC and 7-aminoactinomycin D (7-AAD) (Muse Annexin V and dead cell assay kit, Merck Millipore, U.S.A.). Cells were allowed to be stained with both dyes at room temperature in the dark for 30 min before the samples were subjected to flow cytometry analysis as recommended by the manufacturer. Protein extracts were resolved using precast gradient

SDS-polyacrylamide gel electrophoresis (4−15%, Mini-Protean, Biorad Laboratories Inc., U.S.A.), and electro-transferred onto a nitrocellulose membrane for immunoblot analysis. Specific antibodies were used to detect protein bands in a Chemiluminescence Imaging System (Syngene, U.K.). For apoptotic signaling pathway, TR146 cells were plated overnight on a 6 cm dish with seeding density of 30 000 cells/cm^2. Thereafter, the cells were treated with various concentrations of nano-HA and nano-TiO_2 (0, 62.5, 125, 250, 500, and 1250 μM) for 24 h and cells were lysed using standard Laemmili sample buffer supplemented with 1% protease and phosphatase inhibitors cocktail (Sigma-Aldrich, U.S.A.) and protein expression was analyzed using Western blot technique. The following antibodies were used: anti-phospho p53, anti-total p53, anti-pMDM2, anti-Bax (Cell Signaling Technology, U.S.A.) and anti-β-actin (Santa Cruz Biotechnology, U.S.A.).

2.10. Statistical Analysis. Statistical significance was ascertained using the Origin 9.0 software coupled with Fisher's least significant difference (LSD) post hoc test or Student's t test with data analysis tool of MS EXCEL 2007. p value of <0.05 was considered significant.

3. RESULTS AND DISCUSSION

3.1. Characterization of Pristine NMs. As the size decreases to the nanoscale, additional factors such as structure, size, surface chemistry, and aggregation need to be considered to evaluate the toxicity of the NMs.[19−21] Nano-HA (Figure 1A) and nano-TiO_2 (Figure 1B) were found to be spherical in shape with primary particle sizes of 51.1 ± 12.1 nm and 24.0 ± 7.2 nm, respectively.

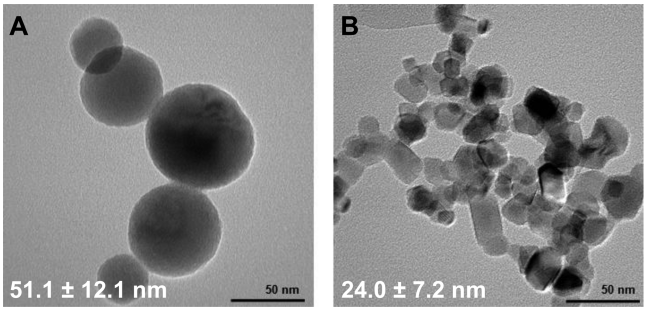

Figure 1. Primary particle size were derived from the TEM images of (A) nano-HA and (B) nano-TiO_2 respectively. (n = 50) Data represent mean ± SD (n = 3).

Next, the hydrodynamic diameter (D_H) and surface charge (ζ-potential) of the NMs were measured in complete cell culture medium so that the actual particle size and surface charge when the NMs interact with the cells could be determined. Despite nano-HA exhibiting an approximately 2 fold larger primary particle size than nano-TiO_2, we noted that upon dispersing in serum containing DMEM/F12 biological medium, both types of NMs formed agglomerates of similar D_H within the range of 280−310 nm. Furthermore, nano-HA and nano-TiO_2 each registered a negative ζ-potential of −5.41 ± 0.59 mV and −7.95 ± 0.76 mV, respectively, which may be attributed to the adsorption of serum derived proteins onto the NMs to form a layer of protein corona.[22]

3.2. Spatial Distribution of Nano-HA and Nano-TiO_2 and in TR146 Human Buccal Epithelial Cells. NMs association, internalization and subcellular localization are key determinants in effecting the biological outcome.[23,24] To gain a better understanding on the rate of NMs uptake, fluorescein isothiocyanate (FITC) green fluorescent dye was covalently conjugated to the surface of nano-HA and nano-TiO_2 to serve as a fluorescent tracker as the NMs interfaces with the cells. FITC immobilization onto the NMs surface was facilitated using APTES to couple the $-NH_2$ group of APTES molecules and the −NCS group of the FITC molecule.

Cell membranes consist of cell receptors that are essential for cell−cell signaling, cell adhesion, and interactions, as well as immune system recognition of foreign substances.[25] Due to the charge density of these NMs, it is possible that they may directly bind to these surface receptors and may have an increased residence time. Biodistribution of FITC conjugated nano-HA and nano-TiO_2 were determined and differences in localization profile between nano-TiO_2 with nano-HA were investigated. At lower concentration (125 μM) of nano-HA, there were almost equal distribution between cytoplasmic and membrane fractions (Figure 2A). However, at a 10-fold higher concentration (1250 μM), there was significant retention of nano-HA in the membrane fraction. This trend was, however, not observed in the nano-TiO_2 treated samples. It could be possible that transmembrane transport of NMs into the cytosol is a size dependent process since more nano-HA was detected in the membrane fraction as opposed to the cytosolic fraction. Cross-sectional confocal acquisition of live cells incubated with the FITC-NMs similarly revealed a higher amount of FITC nano-HA to be located nearer to the apical (top) end of the cells while there is an apparent higher accumulation of FITC-nano TiO_2 nearer to the basolateral (base) end of the cells (Figure 2B). Other studies have shown that NMs of smaller sizes are more likely to be internalized as compared to larger particles.[26,27] Thus, it is probable that majority of the nano-HA, with a larger primary particle size in this study, remained at the peripheral of the cells and limited amount were transported into the cells. Comparatively, the smaller sized nano-TiO_2 was internalized into the cytoplasm. From the particle size perspective, it is likely that the NMs in this study were internalized via caveolae-mediated endocytosis or clathrin-mediated endocytosis, the pathways associated with internalization of particles below 200 nm.[28] However, uptake of NMs via the different endocytic pathways is highly dependent on cell-type; thus, further studies are needed to elucidate the mechanism of how the NMs were internalized into TR146 epithelial cells.

3.3. Nano-HA and Nano-TiO_2 Induced Oxidative Stress and Inflammatory Responses in TR146 Epithelial Cells. The act of brushing breaks up the bacterial biofilms on the surfaces of teeth. Moreover, the nano-sized particles will be able to penetrate deeper into the biofilm to disrupt from within. However, this same mechanism also raised the concern where the amount of ROS generated by these NMs may increase oxidative damage to the oral mucosa with possibly a chronic inflammatory response. There are considerable data that are available to suggest a direct link between ROS production and inflammation.[29] With that backdrop, it was necessary to assess the levels of ROS generated after the NMs were introduced to the cells.

As expected, there was an increased in ROS production with increasing concentrations of nano-HA and nano-TiO_2 particles. All tested concentrations (62.5 to 1250 μM) of nano-HA, a material which is recognized for its biocompatibility (in its micrometer and larger scale), gave rise to the most significant increase in ROS expression levels, with the highest concentration (1250 μM) causing an approximately 40% increase (Figure 3A). In comparison, only the higher concentrations of nano-TiO_2 (250 to 1250 μM) resulted in a significant increase

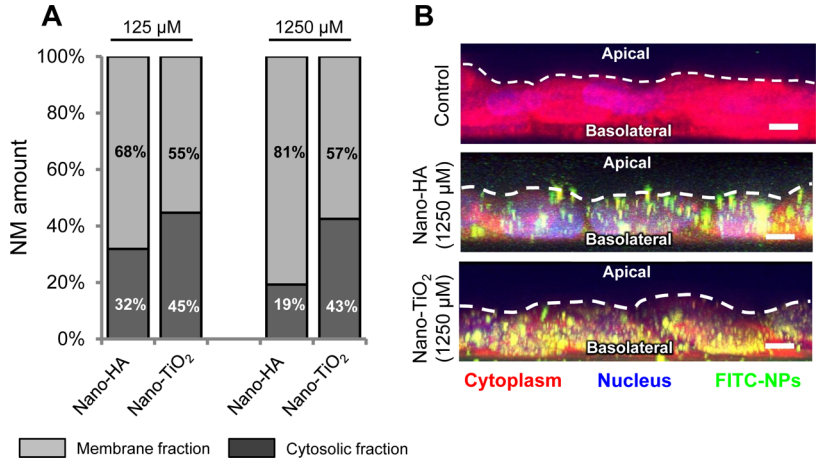

Figure 2. Internalization and subcellular distribution of NMs in TR146 epithelial cells. (A) TR146 epithelial cells were exposed to a low (125 μM) and high (1250 μM) concentration of FITC conjugated nano-HA and nano-TiO_2 for 12 h. Nano-HA displayed higher affinity to the cellular plasma membrane with increasing concentration while subcellular localziation of nano-TiO_2 was found to be independent of NMs concentration. (B) Cross-sectional confocal live imaging of TR146 epithelial cells incubated with 1250 μM of FITC-NMs for 12 h. Data represent mean ± SD (n = 3). Scale bar = 10 μm.

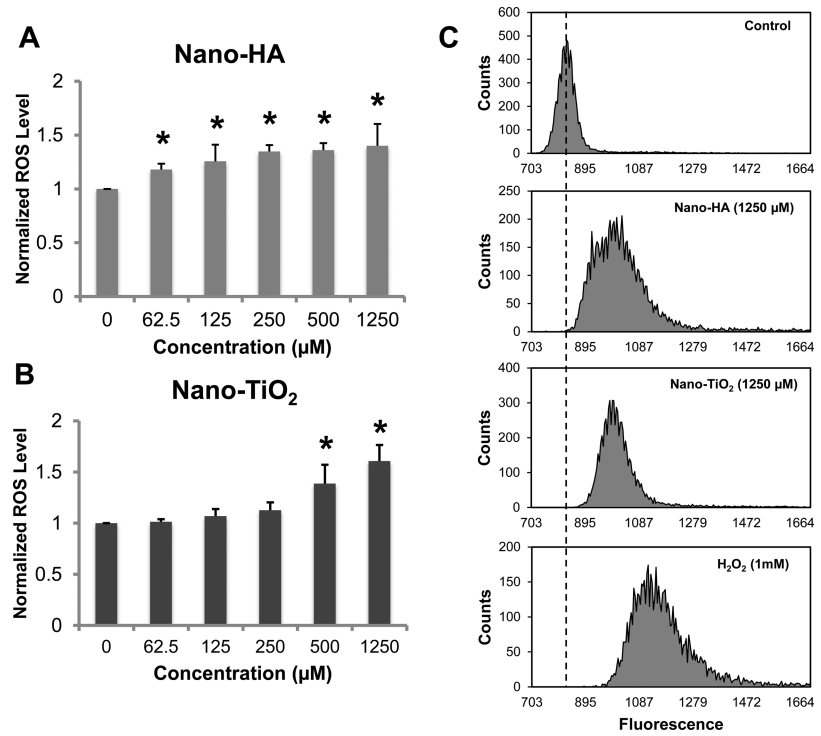

Figure 3. Elevated oxidative status in TR146 epithelial cells following NMs treatment. Intracellular ROS expression of NMs treated cells was detected using DCFH-DA staining and normalized to untreated control. ROS level increases with (A) nano-HA and (B) nano-TiO_2 concentration. Data represent mean ± SD (n = 3). * $p < 0.05$, compared against control. (C) NMs treatment similarly increases mitochondrial specific superoxide level in TR146 epithelial cells. Cells treated with H_2O_2 served as positive control.

in ROS production. Of the two NMs studied, 1250 μM of nano-TiO_2 reflected the highest increase in ROS expression levels—approximately 60% higher compared to the control group (Figure 3B). Consistent with the data derived from the DCFH-DA staining, when the NMs treated cells were counterstained with MitoSox, there is a significant shift in the histogram toward the higher end of the fluorescence spectrum, relative to the untreated control, suggesting that both nano-HA and nano-TiO_2 are able to stimulate mitochondrial superoxide production in TR146 epithelial cells (Figure 3C). Overall, our observations are aligned with other studies whereby nano-HA and nano-TiO_2 were reported to exert their toxic effects through oxidative stress in a dose dependent manner[30−32] and the high surface area: volume ratio of NMs has been reported to potentiate the oxidative stress effect of NMs.[33]

The increase in ROS production suggests that the NMs could potentiate inflammatory response.[34,35] This postulation is in line with the three tiered hierarchical oxidative stress model that was proposed to explained the effects of nanoscale materials on biological systems.[36] The model posits that, prior to a full blown oxidative damage to the cells leading to comprised cell viability (Tier 3), a mild increase in ROS level

dx.doi.org/10.1021/am501266a | ACS Appl. Mater. Interfaces 2014, 6, 6248−6256

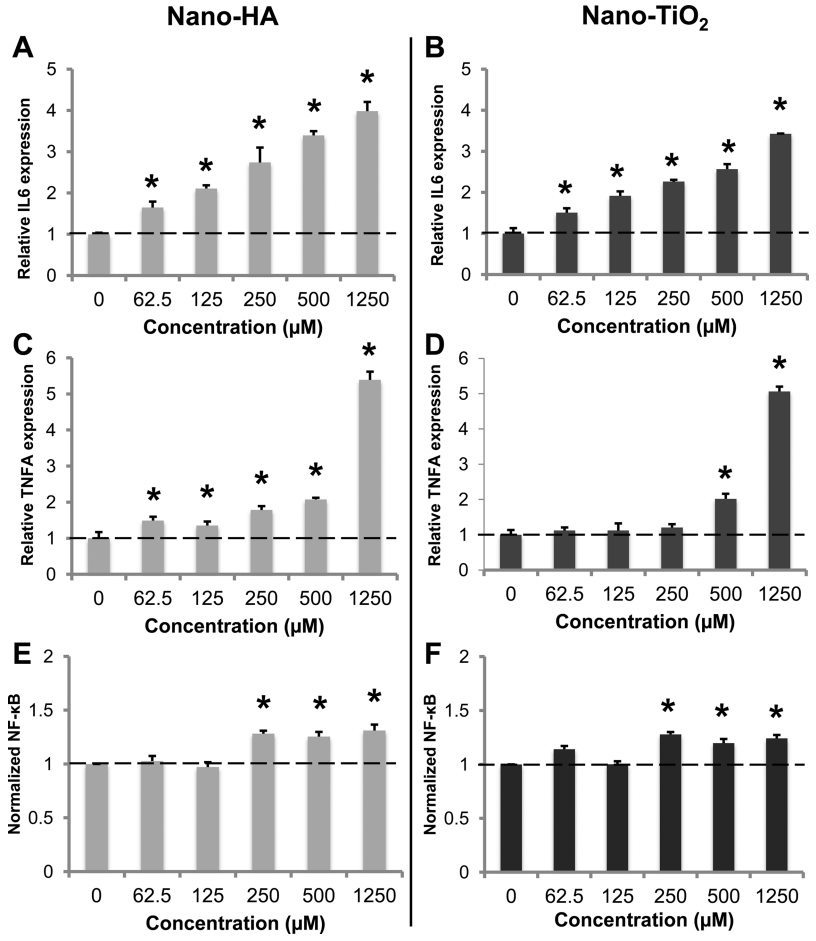

Figure 4. Nano-HA and nano-TiO_2 particles modulate inflammatory response in TR146 epithelial cells and RAW264.7 murine macrophage. RT-PCR was employed to examine inflammatory gene expression in NMs treated samples. Normalized (A and B) IL6 and (C and D) TNFA transcript level for nano-HA and nano-TiO_2 treated samples revealed NMs dose dependent upregulation. Similarly, macrophages treated with both (E) nano-HA and (F) nano-TiO_2 displayed higher expression of NF-κB. Data represent mean ± SD (n = 3). * $p < 0.05$, compared against untreated control.

may instead trigger inflammation.[36] To validate this possibility, we assessed changes in expression level of inflammatory response genes by profiling the expression levels of pro-inflammatory cytokines—specifically Interleukin-6 (IL-6) and tumor necrosis factor-alpha (TNF-α) encoded by the genes IL6 and TNFA, respectively.

We observed a dose dependent elevation in IL6 expression when the cells were treated with nano-HA (Figure 4A). Nano-HA (62.5 to 1250 μM) triggered up to a 4-fold increase of IL6 transcript expression when compared to the untreated control group. Similarly, a trend of increasing concentration of nano-TiO_2 resulted in increasing expression level of IL6 gene. All concentrations of nano-TiO_2 gave rise to significant increase of IL6 expression, with the highest concentration (1250 μM) of nano-TiO_2 giving rise to approximately 3.5-fold increase of IL6 (Figure 4B). Although only concentrations higher than 250 μM of nano-TiO_2 led to a notable increase in ROS production, a significant increase in IL6 expression level was observed for all nano-TiO_2 concentrations. This could possibly be due to the fact that IL6 is also involved in a wider range of cellular and physiological responses.[37] Hence, IL-6 expression alone would not be sufficient to determine if NMs elicited an inflammatory response. As such, expression level of TNFA was also determined. Cells exposed to nano-HA showed a significant increase in expression level of TNFA for all concentrations (62.5 to 1250 μM) of nano-HA (Figure 4C). However, significant up-regulation of TNFA transcript was only observed for concentrations of 500 μM and 1250 μM of nano-TiO_2 (Figure 4D). A 5-fold increase was observed following 1250 μM of nano-HA and nano-TiO_2 treatment.

To further affirm that both nano-HA and nano-TiO_2 are indeed capable of triggering inflammatory response as it interact with the biological system, macrophages transfected with a NF-κB reporter gene, were exposed to various concentrations of nano-HA and nano-TiO_2. NF-κB is an important transcription factor that plays a central role in inflammation due to its ability to induce transcription of pro-inflammatory genes.[34] This reporter indirectly measures the molecules of NF-κB and produces the enzyme luciferase semiquantitatively. After the cells were exposed to the NMs for 6 h, we observed a general trend of elevated expression of NF-κB with increasing concentrations of NMs (Figure 4E and 4F). Lower concentrations (62.5 and 125 μM) of nano-HA did not significantly increase the amount of NF-κB expressed. However, concentrations of more than 250 μM of nano-HA induced approximately 1.2-fold increase in the amount of NF-κB expressed (Figure 4E). Nano-TiO_2 also induced a significant increase in NF-κB expression level. Up to 1.2-fold increase in NF-κB expression was observed when cells were exposed to 1250 μM of nano-TiO_2 (Figure 4F).

3.4. Differential Apoptotic Responses Induced by Nano-TiO_2 and Nano-HA in TR146 Epithelial Cells.

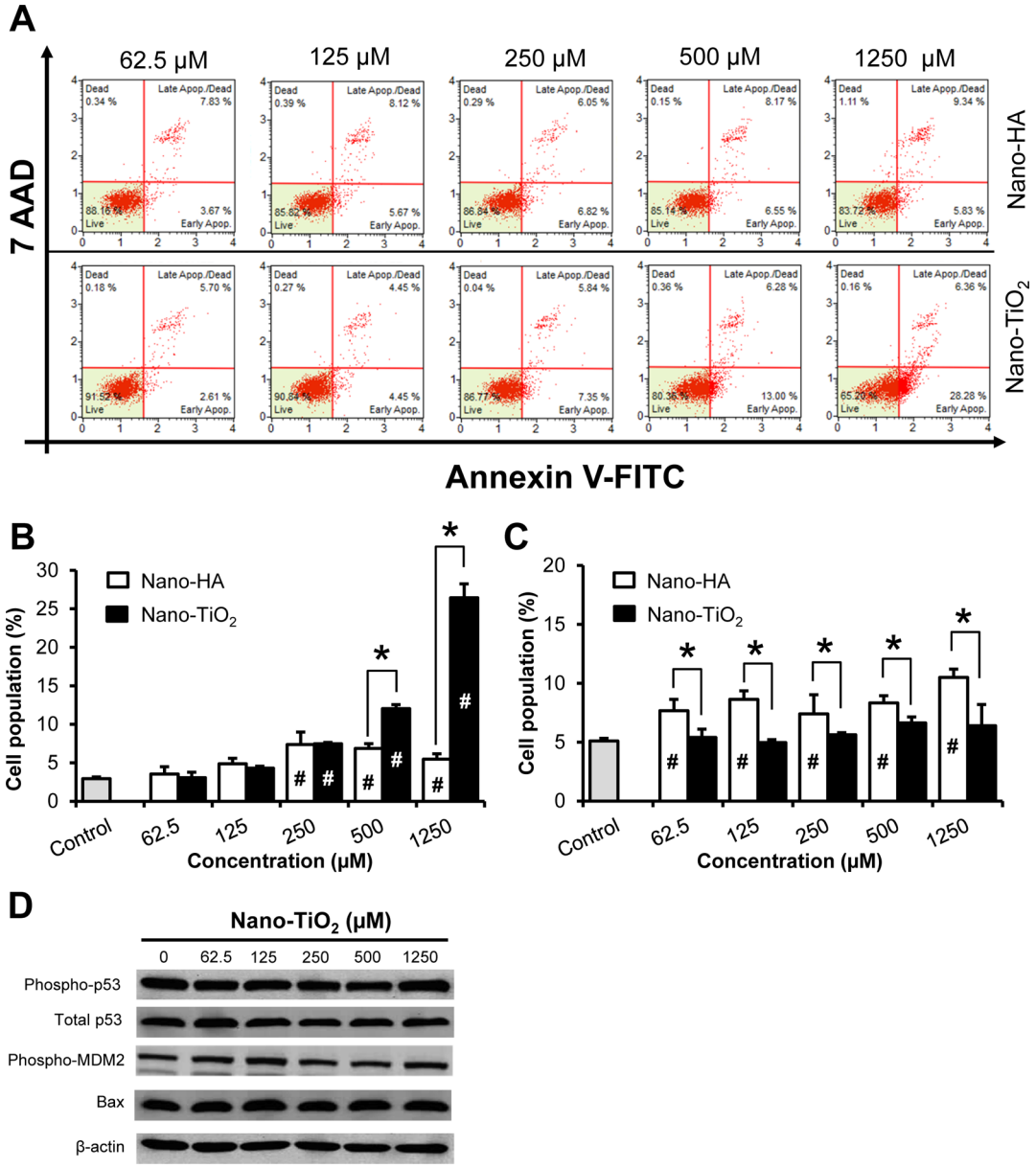

Figure 5. Nano-TiO_2, but not nano-HA, induced early apoptosis in TR146 epithelial cells and is independent of the p53-Bax pathway. (A) Annexin V-FITC/7-AAD scatter plot of TR146 epithelial cells following NMs treatment. Cells were harvested 24 h post NMs treatment and subjected to flow cytometry analysis. A subpopulation of cells following NMs treatment was classified based on the distribution in the scatter plot: Upper left quadrant, necrotic (dead) cells; upper right quadrant, late apoptotic (dead) cells; lower right quadrant, early apoptotic cells; lower left quadrant, viable (live) cells. Subclassification of (B) early and (C) late apoptotic cells following NMs treatment. (D) Western-blot analysis for the p53 mediated extrinsic apoptotic pathway for cells exposed to nano-TiO_2. Data represent mean ± SD ($n = 3$). Statistical significance ($p < 0.05$) is determined by means of one-way ANOVA followed by Fisher's LSD post hoc test. # denotes significant difference compared against control. * denotes significant difference between nano-TiO_2 and nano-HA experimental groups.

Induction of oxidative stress by NMs has also been postulated as a cause for apoptosis.[10,38,39] In view of our previous observations showing that both nano-HA and nano-TiO_2 were able to induce ROS production in TR146 epithelial cells, we ask whether the heightened ROS level may lead to cell apoptosis. Furthermore, substantial uptake of both NM as observed in using confocal microscopy (Figure 2) may also potentially elevate intracellular calcium concentration, leading to dysregulation of cell function and cell death.[40] Cells were exposed to predetermined concentrations of pristine nano-HA and nano-TiO_2 particles and percentage of apoptotic cells was determined by flow cytometry following annexin-V/7-aminoactinomycin D (7-AAD) staining (Figure 5A). Cells undergoing early apoptosis are characterized by translocation of phosphatidylserine (PS) to the extracellular membrane, which can be detected using annexin-V. During late stage apoptosis, in addition to the expression of PS at the surface of the cell membrane, integrity of the cellular membrane is also comprised and thus facilitates infiltration of the 7-AAD nucleic acid dye. In contrast, cells that were not stained were identified as viable cells and cells stained only with 7-AAD denotes necrotic cells. Several major findings were made. First, we noted that cells treated with both NMs retained high cell viability >90% and percentage of necrotic cells did not fluctuate even at high NMs exposure. Comparing

dx.doi.org/10.1021/am501266a | ACS Appl. Mater. Interfaces 2014, 6, 6248−6256

nano-TiO_2 and nano-HA treated samples, nano-TiO_2 treatment clearly induces a higher percent of early apoptotic cells in a dose dependent manner (Figure 5B). Specifically, the untreated control sample registered 2.8% of early apoptotic cells whereas samples spiked with 1250 μM of nano-TiO_2 registered approximately 28% of cells undergoing early apoptosis suggesting that the apoptotic program has been initiated with nano-TiO_2 treatment. In stark contrast, nano-HA treated samples at concentration of 250 μM and beyond displayed only a modest increase in early apoptotic cells by approximately 4% (Figure 5B). Interestingly, cells treated with nano-HA, however, consistently exhibited significant increase in percentage of late apoptotic cells by almost 2 fold compared to the untreated control (Figure 5C). Conversely, the number of cells in late apoptosis was relatively constant and is not significantly different from the control group even at high concentration of nano-TiO_2. Taking reference to Figure 2, which shows a high amount of nano-HA residing at the membrane fraction, it is likely that nano-HA may interferes with the lipid bilayer and thus induces apoptosis through damage to the cell membrane. On the other hand, nano-TiO_2 was observed to have a higher cytoplasmic localization and may trigger a defensive move by the cell to isolate these foreign entity until a critical threshold is reached, beyond which, the apoptotic events cannot be prevented anymore. In this context, comparing both nano-HA and nano-TiO_2, one would therefore anticipate the existence of some degree of temporal lag for the trigger of apoptosis in both cases.

To gain further insights into the underlying mechanism by which nano-TiO_2 could possibly induce apoptotic event in TR146 epithelial cells, we examined the p53-mediated intrinsic apoptosis pathway that had been shown to be involved in nano-TiO_2 induced apoptosis. Previous studies have shown that nano-TiO_2 along with other metal oxide NMs can trigger DNA damage,[41−45] which is regulated by the tumor suppressor protein, p53. Specifically, Yoo et al.[10] provided evidence of perturbed p53 activity in MCF10A and WI38 human cell lines in response to P25 nano-TiO_2 treatment via a ROS dependent mechanism. Surprisingly, we did not observe any increase in phosphorylation of MDM2 with increasing concentrations of nano-TiO_2 treated cells. Phosphorylated MDM2 leads to the degradation of p53.[46,47] Therefore, the lack of changes to the expression levels of phosphorylated MDM2, phosphorylated p53, and total p53 levels (Figure 5D) implied there is no significant activation of the DNA damage response above the basal levels of the p53 protein. Bcl-2-associated X protein (Bax) protein is a downstream target of the p53 that has a pro apoptotic function by translocating into the mitochondria, leading to the activation of mitochondrial stress related proteins and apoptosis.[48] Consistently, there was no significant difference between expression levels of Bax between the nano-TiO_2 treated cells and control cells. In agreement with our observations, the lack of classical p53-Bax apoptotic signaling cascade involvement in nano-TiO_2 mediated programmed cell death was also recently demonstrated using $BAK^{-/-}BAX^{-/-}$ cell lines.[49] It is therefore possible that the levels of ROS may have resulted in significant levels of lipid peroxidation that led to lysosomal membrane destabilizing and thus leading to cathespin B release and subsequent activation of caspases and finally apoptosis—independent of p53.[50]

4. CONCLUSION

Despite the lack of understanding on the nature of interaction of manufactured NMs with biological systems, the production and incorporation of these NMs in a plethora of commercial products continue to grow at an alarming scale. Furthermore, the rapid advancement in nanotechnology has also provided the technological means to produce a wide range of "exotic" NMs with unique electrical, optical, biological, and chemical properties that will undoubtedly yield numerous technological benefits and their applications are expected to swell in years to come. It is therefore of paramount importance that the potential risks of using these manufactured NMs should be evaluated, so as to ensure their safe usage. In this study, using commercially available nano-HA (~51 nm) and nano-TiO_2 (~24 nm) as model manufactured NMs found in numerous off-the-shelf products such as toothpastes, we examined the uptake, subcellular localization, oxidative stress, inflammatory, and apoptotic responses in human TR146 oral muccosa buccal epithelial cells. The major findings made in this study are summarized in Figure 6. Specifically, we noted that cell uptake,

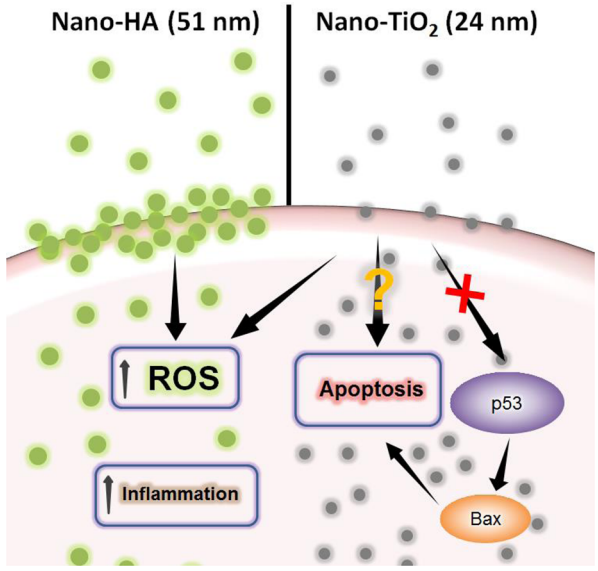

Figure 6. Tale of differential cellular responses elicited by nano-HA and nano-TiO_2 in human oral epithelial cells. Unlike nano-TiO_2, nano-HA accumulates predominately at or near the cell membrane. Both NMs were able to induce oxidative stress in TR146 epithelial cells along with increased expression of inflammatory genes such as IL6 and TNFA. However, only cells treated with nano-TiO_2 underwent significant apoptosis, independent of the p53-Bax pathway.

subcellular localization, ROS production, inflammatory responses, and induction of early apoptotic events varies accordingly to the chemical nature of NMs. Compared to nano-TiO_2, nano-HA displayed preferential accumulation proximal to the cell membrane. In addition, we observed a good correlation between the NMs induced elevated intracellular ROS level and upregulation of inflammatory genes such as IL6 and TNFA. Consistent with this findings, murine macrophage similarly expresses more NF-κB under the influence of both NMs which further substantiated the pro-inflammatory action of nano-HA and nano-TiO_2. Percentage of early apoptotic cells increased with nano-TiO_2 dosage by the end of 24 h treatment, suggesting that the apoptotic machinery had been initiated. Further analysis of the signaling proteins

expression by use immunoblotting indicated that nano-TiO_2 triggered apoptosis is independent of the classical p53-Bax apoptosis signaling, suggesting the existence of a novel nano-TiO_2 specific apoptotic mechanism that may be implicated.

AUTHOR INFORMATION

Corresponding Authors

* Email: cheltwd@nus.edu.sg.
* Email: denchhl@nus.edu.sg.

Author Contributions

[§]D.T.L. conceived the hypotheses. C.Y.T., W.F., S.L.C., and M.I.S. performed all the experiments. K.S.T., C.H.L.H., C.Y.T., W.F., and D.T.L. conceived the experimental design and analyzed the data. C.Y.T., W.F., C.H.L.H., and D.T.L. wrote the manuscript. C.Y.T. and W.F. contributed equally to the work.

Notes

The authors declare no competing financial interest.

ACKNOWLEDGMENTS

This study was supported by Ministry of Education Academic Research Grants (R-279-000-350-112 to D.T.L) and the Faculty of Engineering Strategic Research Fund (R-397-000-136-112). C.Y.T acknowledged support from the Lee Kuan Yew Postdoctoral Fellowship.

REFERENCES

(1) Wu, Y. L.; Putcha, N.; Ng, K. W.; Leong, D. T.; Lim, C. T.; Loo, S. C. J.; Chen, X. Biophysical Responses Upon the Interaction of Nanomaterials with Cellular Interfaces. *Acc. Chem. Res.* **2012**, *46*, 782−791.

(2) Setyawati, M. I.; Fang, W.; Chia, S. L.; Leong, D. T. Nanotoxicology of Common Metal Oxide Based Nanomaterials: Their ROS-y and Non-ROS-y Consequences. *Asia-Pac. J. Chem. Eng.* **2013**, *8*, 205−217.

(3) Setyawati, M. I.; Tay, C. Y.; Leong, D. T. Effect of Zinc Oxide Nanomaterials-Induced Oxidative Stress on the p53 Pathway. *Biomaterials* **2013**, *34*, 10133−10142.

(4) Tay, C. Y.; Cai, P.; Setyawati, M. I.; Fang, W.; Tan, L. P.; Hong, C. H. L.; Chen, X.; Leong, D. T. Nanoparticles Strengthen Intracellular Tension and Retard Cellular Migration. *Nano Lett.* **2013**, *14*, 83−88.

(5) Setyawati, M. I.; Tay, C. Y.; Leong, D. T. W. Exploiting Cancer's Anti-oxidative Weakness through p53 with Nanotoxicology. *Nanomedicine* **2014**, DOI: 10.2217/NNM.14.6.

(6) Hannig, M.; Hannig, C. Nanomaterials in Preventive Dentistry. *Nat. Nanotechnol.* **2010**, *5*, 565−569.

(7) Tian, K.; Peng, M.; Ren, X.; Liao, C.; Fei, W. Regeneration of Tooth-like Hydroxyapatite Depended on Amelogenin Functional Section Monolayer: A New Approach for Tooth Repair. *Med. Hypotheses* **2012**, *79*, 143−146.

(8) Niwa, M.; Sato, T.; Li, W.; Aoki, H.; Aoki, H.; Daisaku, T. Polishing and Whitening Properties of Toothpaste Containing Hydroxyapatite. *J. Mater. Sci.: Mater. Med.* **2001**, *12*, 277−281.

(9) Zhao, X.; Heng, B. C.; Xiong, S.; Guo, J.; Tan, T. T.; Boey, F. Y.; Ng, K. W.; Loo, J. S. In vitro Assessment of Cellular Responses to Rod-Shaped Hydroxyapatite Nanoparticles of Varying Lengths and Surface Areas. *Nanotoxicology* **2011**, *5*, 182−194.

(10) Yoo, K. C.; Yoon, C. H.; Kwon, D.; Hyun, K. H.; Woo, S. J.; Kim, R. K.; Lim, E. J.; Suh, Y.; Kim, M. J.; Yoon, T. H.; Lee, S. J. Titanium Dioxide Induces Apoptotic Cell Death Through Reactive Oxygen Species-Mediated Fas Upregulation and Bax Activation. *Int. J. Nanomed.* **2012**, *7*, 1203−1214.

(11) Xiong, S.; Tang, Y.; Ng, H. S.; Zhao, X.; Jiang, Z.; Chen, Z.; Ng, K. W.; Loo, S. C. Specific Surface Area of Titanium Dioxide (TiO_2) Particles Influences Cyto- and Photo-Toxicity. *Toxicology* **2013**, *304*, 132−140.

(12) Park, E. J.; Yoon, J.; Choi, K.; Yi, J.; Park, K. Induction of Chronic Inflammation in Mice Treated with Titanium Dioxide Nanoparticles by Intratracheal Instillation. *Toxicology* **2009**, *260*, 37−46.

(13) Howie, N. M.; Trigkas, T. K.; Cruchley, A. T.; Wertz, P. W.; Squier, C. A.; Williams, D. M. Short-Term Exposure to Alcohol Increases the Permeability of Human Oral Mucosa. *Oral Dis.* **2001**, *7*, 349−354.

(14) Herlofson, B. B.; Barkvoll, P. Desquamative Effect of Sodium Lauryl Sulfate on Oral Mucosa. A Preliminary Study. *Acta Odontol. Scand.* **1993**, *51*, 39−43.

(15) Gopee, N. V.; Roberts, D. W.; Webb, P.; Cozart, C. R.; Siitonen, P. H.; Latendresse, J. R.; Warbitton, A. R.; Yu, W. W.; Colvin, V. L.; Walker, N. J.; Howard, P. C. Quantitative Determination of Skin Penetration of PEG-Coated CdSe Quantum Dots in Dermabraded but Not Intact SKH-1 Hairless Mouse Skin. *Toxicol. Sci.* **2009**, *111*, 37−48.

(16) Oberdorster, G.; Oberdorster, E.; Oberdorster, J. Nanotoxicology: An Emerging Discipline Evolving from Studies of Ultrafine Particles. *Environ. Health Perspect.* **2005**, *113*, 823−839.

(17) Setyawati, M. I.; Tay, C. Y.; Chia, S. L.; Goh, S. L.; Fang, W.; Neo, M. J.; Chong, H. C.; Tan, S. M.; Loo, S. C.; Ng, K. W.; Xie, J. P.; Ong, C. N.; Tan, N. S.; Leong, D. T. Titanium Dioxide Nanomaterials Cause Endothelial Cell Leakiness by Disrupting the Homophilic Interaction of VE-cadherin. *Nat. Commun.* **2013**, *4*, 1673.

(18) Weir, A.; Westerhoff, P.; Fabricius, L.; Hristovski, K.; von Goetz, N. Titanium Dioxide Nanoparticles in Food and Personal Care Products. *Environ. Sci. Technol.* **2012**, *46*, 2242−2250.

(19) Ding, Y.; Bian, X.; Yao, W.; Li, R.; Ding, D.; Hu, Y.; Jiang, X.; Hu, Y. Surface-Potential-Regulated Transmembrane and Cytotoxicity of Chitosan/Gold Hybrid Nanospheres. *ACS Appl. Mater. Interfaces* **2010**, *2*, 1456−1465.

(20) Yan, L.; Zhao, F.; Li, S.; Hu, Z.; Zhao, Y. Low-Toxic and Safe Nanomaterials by Surface-Chemical Design, Carbon Nanotubes, Fullerenes, Metallofullerenes, and Graphenes. *Nanoscale* **2011**, *3*, 362−382.

(21) Liao, K.-H.; Lin, Y.-S.; Macosko, C. W.; Haynes, C. L. Cytotoxicity of Graphene Oxide and Graphene in Human Erythrocytes and Skin Fibroblasts. *ACS Appl. Mater. Interfaces* **2011**, *3*, 2607−2615.

(22) Lundqvist, M.; Stigler, J.; Elia, G.; Lynch, I.; Cedervall, T.; Dawson, K. A. Nanoparticle Size and Surface Properties Determine the Protein Corona with Possible Implications for Biological Impacts. *Proc. Natl. Acad. Sci. U.S.A.* **2008**, *105*, 14265−14270.

(23) Chen, N.; He, Y.; Su, Y.; Li, X.; Huang, Q.; Wang, H.; Zhang, X.; Tai, R.; Fan, C. The Cytotoxicity of Cadmium-Based Quantum Dots. *Biomaterials* **2012**, *33*, 1238−1244.

(24) Tay, C. Y.; Yu, Y.; Setyawati, M. I.; Xie, J.; Leong, D. T. Presentation Matters: Identity of Gold Nanoclusters Capping Agent Governs Intracellular Uptake and Cell Metabolism. *Nano Res.* **2014**, DOI: 10.1007/s12274-014-0441-z.

(25) Naka, T.; Nishimoto, N.; Kishimoto, T. The Paradigm of IL-6: From Basic Science to Medicine. *Arthritis Res.* **2002**, *4*, S233−S242.

(26) Chithrani, B. D.; Chan, W. C. W. Elucidating the Mechanism of Cellular Uptake and Removal of Protein-Coated Gold Nanoparticles of Different Sizes and Shapes. *Nano Lett.* **2007**, *7*, 1542−1550.

(27) Jiang, W.; Kim, B. Y.; Rutka, J. T.; Chan, W. C. Nanoparticle-Mediated Cellular Response is Size-Dependent. *Nat. Nanotechnol.* **2008**, *3*, 145−150.

(28) Vercauteren, D.; Vandenbroucke, R. E.; Jones, A. T.; Rejman, J.; Demeester, J.; De Smedt, S. C.; Sanders, N. N.; Braeckmans, K. The Use of Inhibitors to Study Endocytic Pathways of Gene Carriers: Optimization and Pitfalls. *Mol. Ther.* **2010**, *18*, 561−569.

(29) Nathan, C.; Cunningham-Bussel, A. Beyond Oxidative Stress: An Immunologist's Guide to Reactive Oxygen Species. *Nat. Rev. Immunol.* **2013**, *13*, 349−361.

(30) Meena, R.; Kesari, K.; Rani, M.; Paulraj, R. Effects of Hydroxyapatite Nanoparticles on Proliferation and Apoptosis of Human Breast Cancer Cells (MCF-7). *J. Nanopart. Res.* **2012**, *14*, 1−11.

(31) Park, E. J.; Yi, J.; Chung, K. H.; Ryu, D. Y.; Choi, J.; Park, K. Oxidative Stress and Apoptosis Induced by Titanium Dioxide Nanoparticles in Cultured BEAS-2B Cells. *Toxicol. Lett.* **2008**, *180*, 222−229.
(32) Yang, H.; Liu, C.; Yang, D.; Zhang, H.; Xi, Z. Comparative Study of Cytotoxicity, Oxidative Stress, and Genotoxicity Induced by Four Typical Nanomaterials: The Role of Particle Size, Shape, and Composition. *J. Appl. Toxicol.* **2009**, *29*, 69−78.
(33) Donaldson, K.; Stone, V.; Tran, C. L.; Kreyling, W.; Borm, P. J. Nanotoxicology. *Occup. Environ. Med.* **2004**, *61*, 727−728.
(34) Tay, C. Y.; Fang, W.; Setyawati, M. I.; Sum, C. P.; Xie, J.; Ng, K. W.; Chen, X.; Hong, C. H. L.; Leong, D. T. Reciprocal Response of Human Oral Epithelial Cells to Internalized Silica Nanoparticles. *Part. Part. Syst. Charact.* **2013**, *30*, 784−793.
(35) Khodr, B.; Khalil, Z. Modulation of Inflammation by Reactive Oxygen Species: Implications for Aging and Tissue Repair. *Free Radical Biol. Med.* **2001**, *30*, 1−8.
(36) Nel, A.; Xia, T.; Mädler, L.; Li, N. Toxic Potential of Materials at the Nanolevel. *Science* **2006**, *311*, 622−627.
(37) Tak, P. P.; Firestein, G. S. NF-κB: A Key Role in Inflammatory Diseases. *J. Clin. Invest.* **2001**, *107*, 7−11.
(38) Cheng, X.; Zhang, W.; Ji, Y.; Meng, J.; Guo, H.; Liu, J.; Wu, X.; Xu, H. Revealing Silver Cytotoxicity Using Au Nanorods/Ag Shell Nanostructures: Disrupting Cell Membrane and Causing Apoptosis Through Oxidative Damage. *RSC Adv.* **2013**, *3*, 2296−2305.
(39) Joris, F.; Manshian, B. B.; Peynshaert, K.; De Smedt, S. C.; Braeckmans, K.; Soenen, S. J. Assessing Nanoparticle Toxicity in Cell-Based Assays: Influence of Cell Culture Parameters and Optimized Models for Bridging the In Vitro−In Vivo Gap. *Chem. Soc. Rev.* **2013**, *42*, 8339−8359.
(40) Tang, W.; Yuan, Y.; Liu, C.; Wu, Y.; Lu, X.; Qian, J. Differential Cytotoxicity and Particle Action of Hydroxyapatite Nanoparticles in Human Cancer Cells. *Nanomedicine* **2013**, 1−15, DOI: 10.2217/nnm.12.217.
(41) Nabeshi, H.; Yoshikawa, T.; Matsuyama, K.; Nakazato, Y.; Tochigi, S.; Kondoh, S.; Hirai, T.; Akase, T.; Nagano, K.; Abe, Y.; Yoshioka, Y.; Kamada, H.; Itoh, N.; Tsunoda, S.-i.; Tsutsumi, Y. Amorphous Nanosilica Induce Endocytosis-Dependent ROS Generation and DNA Damage in Human Keratinocytes. *Part. Fibre Toxicol.* **2011**, *8*, 1.
(42) Sanpui, P.; Chattopadhyay, A.; Ghosh, S. S. Induction of Apoptosis in Cancer Cells at Low Silver Nanoparticle Concentrations Using Chitosan Nanocarrier. *ACS Appl. Mater. Interfaces* **2011**, *3*, 218−228.
(43) Setyawati, M. I.; Khoo, P. K.; Eng, B. H.; Xiong, S.; Zhao, X.; Das, G. K.; Tan, T. T.; Loo, J. S.; Leong, D. T.; Ng, K. W. Cytotoxic and Genotoxic Characterization of Titanium Dioxide, Gadolinium Oxide, and Poly(lactic-co-glycolic acid) Nanoparticles in Human Fibroblasts. *J. Biomed. Mater. Res., Part A* **2013**, *101A*, 633−640.
(44) Singh, S.; D'Britto, V.; Prabhune, A. A.; Ramana, C. V.; Dhawan, A.; Prasad, B. L. V. Cytotoxic and Genotoxic Assessment of Glycolipid-Reduced and -Capped Gold and Silver Nanoparticles. *New J. Chem.* **2010**, *34*, 294−301.
(45) Ng, K. W.; Khoo, S. P.; Heng, B. C.; Setyawati, M. I.; Tan, E. C.; Zhao, X.; Xiong, S.; Fang, W.; Leong, D. T.; Loo, J. S. The Role of the Tumor Suppressor p53 Pathway in the Cellular DNA Damage Response to Zinc Oxide Nanoparticles. *Biomaterials* **2011**, *32*, 8218−8225.
(46) Haupt, Y.; Maya, R.; Kazaz, A.; Oren, M. Mdm2 Promotes the Rapid Degradation of p53. *Nature* **1997**, *387*, 296−299.
(47) Jennings, P.; Limonciel, A.; Felice, L.; Leonard, M. O. An Overview of Transcriptional Regulation in Response to Toxicological Insult. *Arch. Toxicol.* **2013**, *87*, 49−72.
(48) Fulda, S.; Debatin, K. M. Extrinsic Versus Intrinsic Apoptosis Pathways in Anticancer Chemotherapy. *Oncogene* **2006**, *25*, 4798−4811.
(49) Zhu, Y.; Eaton, J. W.; Li, C. Titanium Dioxide (TiO_2) Nanoparticles Preferentially Induce Cell Death in Transformed Cells in A Bak/Bax-Independent Fashion. *PLoS One* **2012**, *7*, e50607.
(50) Hussain, S.; Thomassen, L. C.; Ferecatu, I.; Borot, M. C.; Andreau, K.; Martens, J. A.; Fleury, J.; Baeza-Squiban, A.; Marano, F.; Boland, S. Carbon Black and Titanium Dioxide Nanoparticles Elicit Distinct Apoptotic Pathways in Bronchial Epithelial Cells. *Part. Fibre Toxicol.* **2010**, *7*, 10.